




Cite this: *RSC Adv.*, 2025, 15, 8262

# Unveiling electronic and remarkable non-linear optical properties of boron–nitrogen carbazole-based compounds *via* modification of $\pi$ -linker and donor units: a DFT study†

Sadia Jamal,<sup>a</sup> Nadeem Raza,<sup>b</sup> Muhammad Khalid <sup>\*a</sup>  
and Ataulpa Albert Carmo Braga <sup>c</sup>

Boron–nitrogen carbazole (BNCz) based aromatic chromophores have been considered as promising materials in non-linear optical domains due to their distinctive electronic and charge-transfer capabilities. This study presents the electronic and non-linear optical properties of BNCz-based compounds (BTNC–BNPZ). Additionally, a new series of four BNCz-based compounds (BNTP–BNTQ) with D– $\pi$ –A framework was designed by modifying the donors and  $\pi$ -spacer. Structural optimization and optoelectronic properties of BNCz based compounds were determined using density functional theory/time-dependent density functional theory (DFT/TD-DFT) calculations at M06/6-311G(d,p) level. The optimized structures were used to perform frontier molecular orbitals (FMOs), density of states (DOS), transition density matrix (TDM), UV-Visible and non-linear optical (NLO) analyses of examined compounds. The red-shifted absorption spectrum (412.854–566.138 nm) combined with a suitable energy gap (2.784–3.774 eV) facilitates significant charge migration from HOMO to LUMO. The global reactivity descriptors revealed notable softness and significant chemical reactivity in all above-mentioned chromophores. Among all the studied compounds, BNPZ displayed the narrowest band gap (2.784 eV), the highest absorption peak (566.138 nm), and lowest excitation energy (2.190 eV), highlighting its remarkable electronic characteristics. Furthermore, DOS visualizations and TDM heat maps support the FMO findings, confirming the presence of charge densities in a chromophore. All the compounds showed an increased exciton dissociation rate due to their lower exciton binding energy values ( $E_b$  = 0.771–0.480 eV). Moreover, NBO analysis revealed that enhanced hyperconjugation and strong intramolecular interactions played a crucial role in stabilizing the studied compounds. Among all the derivatives, BNTP exhibited the highest  $\beta_{tot}$  ( $74.0 \times 10^{-30}$  esu) and  $\gamma_{tot}$  ( $81.1 \times 10^{-35}$  esu) values, suggesting its promising potential as an NLO material.

Received 5th February 2025  
Accepted 11th March 2025

DOI: 10.1039/d5ra00864f

rsc.li/rsc-advances

## Introduction

Nonlinear optical (NLO) materials have gained significant strides in recent decades particularly in fiber optics, photonic lasers, and data storage for wireless communication systems.<sup>1</sup> These developments have profoundly influenced data processing and related technologies. Both organic and inorganic NLO materials have emerged as crucial and challenging areas of

research.<sup>2</sup> Inorganic materials have long dominated the commercial NLO applications due to their unique optical properties, high thermal stability, and efficient second-harmonic generation (SHG).<sup>3</sup> However, the past fifteen years have witnessed a growing focus on organic systems driven by their structural versatility and tunable properties.<sup>4</sup> Organic NLO materials present several advantages, including high absorption efficiency, strong NLO susceptibilities, and excellent thermal stability. Their  $\pi$ -electron delocalization enables rapid response times, contributing to outstanding NLO performance. Initially, organic compounds were often paired with fullerene-derived acceptor units to enhance charge transfer capabilities. However, fullerene-based systems have notable drawbacks, such as high production costs, limited visible-light absorption, challenges in energy-level tuning, and poor photostability.<sup>5</sup> Consequently, researchers have shifted toward non-fullerene (NF) chromophores, which offer cost-effective synthesis and

<sup>a</sup>Institute of Chemistry, Khwaja Fareed University of Engineering & Information Technology, Rahim Yar Khan, 64200, Pakistan

<sup>b</sup>Department of Chemistry, College of Science, Imam Mohammad Ibn Saud Islamic University (IMSIU), Riyadh, Saudi Arabia. E-mail: nrmostafa@imamu.edu.sa

<sup>c</sup>Departamento de Química Fundamental, Instituto de Química, Universidade de São Paulo, Av. Prof. Lineu Prestes, 748, São Paulo, 05508-000, Brazil. E-mail: muhammad.khalid@kfueit.edu.pk; khalid@iq.usp.br

† Electronic supplementary information (ESI) available. See DOI: <https://doi.org/10.1039/d5ra00864f>


enable precise tuning of chemical structures and energy levels.<sup>6</sup> Moreover, NF-based compounds offer exceptional stability and allow for easy modulation of electronic and optical properties through structural modifications.<sup>7</sup> Therefore, understanding the molecular structure in detail is crucial for uncovering the interconnections between different components of the investigated compounds.<sup>8</sup> Key NLO characteristics, such as orbital energy gaps, migration of electrons *via*  $\pi$ -linkers, dipole moment variations, and excited state transitions, can be optimized through structural modeling.<sup>9</sup> Various push pull strategies, including donor-acceptor, donor- $\pi$ -acceptor, acceptor- $\pi$ -donor- $\pi$ -acceptor, donor- $\pi$ - $\pi$ -acceptor, and donor-donor- $\pi$ -acceptor, have been widely explored. Studies demonstrate that organic frameworks exhibit remarkable NLO performance through the push-pull (D- $\pi$ -A) model, sparking significant interest in such chromophores.<sup>10</sup> The nature of donor and acceptor functions along with the extent of  $\pi$ -conjugation also play a crucial role in determining NLO properties, primarily *via* intramolecular charge transfer (ICT).<sup>11</sup> The BNCz core, with its tricoordinate boron atoms, exhibits strong electron-accepting properties, while functionalization with aryl groups stabilizes the structure and fine-tunes electronic properties for enhanced NLO performance.<sup>12</sup> Additionally, the phenylthiophene  $\pi$ -spacer is expected to effectively enhance conjugation, further optimizing the charge transfer and NLO efficiency.<sup>13</sup>

Building on these considerations, this study presents NLO analysis of four boron-nitrogen carbazole (BNCz) based compounds, synthesized *via* nucleophilic aromatic substitution and electrophilic arene borylation as reported by Hui He and colleagues.<sup>14</sup> Additionally, four new BNCz based derivatives, featuring a phenyl thiophene  $\pi$ -spacer and strong phenazine based donor groups were designed. A DFT based investigation was conducted to evaluate the impact of  $\pi$ -linker and donor variations on the NLO properties, assessing the potential of these compounds for practical NLO applications.

## Computational procedure

All the calculations for current study were conducted using Gaussian 16 software package.<sup>15</sup> DFT and TD-DFT investigations were performed at M06 level 6-311G(d,p) and basis set to explore the electronic and NLO properties of **BTNC-BNPZ** and **BNTP-BNTO**. At first, the geometries of these chromophores were optimized at the ground state using abovementioned functional, then these optimized structures were utilized for further analyses. The UV-Visible spectra, frontier molecular orbital, transition density matrix were carried out using the TD-DFT method whereas NBOs, DOS and NLO analyses were conducted at DFT approach. To investigate the stabilization patterns of entitled compounds NBO study was performed. Avogadro software<sup>16</sup> was utilized to calculate the FMOs energies and developed their counter surfaces to illustrate the charge transfer in entitled chromophores. The chemical reactivity of **BTNC-BNPZ** and **BNTP-BNTO** was assessed by calculating their global reactivity descriptors (GRDs) with the aid of valence and conduction energy gaps. The quantitative assessment of electronic cloud at various parts of studied D-A and D- $\pi$ -A

chromophores was conducted through DOS analysis to support the insights gained from FMOs. Several software tools, *i.e.*, GaussSum,<sup>17</sup> Chemcraft,<sup>18</sup> Multiwfn,<sup>19</sup> and Gauss View 5.0,<sup>20</sup> were employed to get the information from the output files. Eqn (1)–(4) were applied to determine values of dipole moment ( $\mu$ ),<sup>21</sup> linear polarizability  $\alpha$ ,<sup>22</sup> the first hyperpolarizability ( $\beta_{\text{total}}$ ),<sup>23</sup> and second hyperpolarizability ( $\gamma_{\text{total}}$ ).<sup>24</sup>

$$\mu = (\mu_x^2 + \mu_y^2 + \mu_z^2)^{1/2} \quad (1)$$

$$\langle \alpha \rangle = (a_{xx} + a_{yy} + a_{zz})/3 \quad (2)$$

$$\beta_{\text{total}} = (\beta_x^2 + \beta_y^2 + \beta_z^2)^{1/2} \quad (3)$$

whereas  $\beta_x = \beta_{xxx} + \beta_{xyy} + \beta_{xzz}$ ,  $\beta_y = \beta_{yxx} + \beta_{yyy} + \beta_{yzz}$  and  $\beta_z = \beta_{zxx} + \beta_{zyy} + \beta_{zzz}$

$$\gamma_{\text{total}} = \sqrt{\gamma_x^2 + \gamma_y^2 + \gamma_z^2} \quad (4)$$

whereas  $\gamma_i = \frac{1}{15} \sum_j (\gamma_{ijji} + \gamma_{ijjj} + \gamma_{ijjj})$   $i, j = \{x, y, z\}$

## Results and discussion

This study investigates the NLO properties of four previously synthesized boron-nitrogen-based compounds<sup>14</sup> (**BTNC**, **BNAC**, **BNPZ**, and **BNPZ**) featuring a BNCz acceptor core with various donor units. To optimize computational efficiency and reduce steric hindrance, longer alkyl chains in these compounds were replaced with shorter methyl groups. Additionally, four newly designed BNCz-based derivatives (**BNTP**, **BNTC**, **BNTA**, and **BNTO**) were also designed, incorporating a D- $\pi$ -A framework with a 2-phenylthiophene  $\pi$ -bridge and efficient donor groups (Fig. 1). The structures and IUPAC names of the utilized donor groups for entitled compounds are provided in Table S32.† The ground state geometries of the aforesaid compounds are depicted in Fig. 2, with Chemdraw structures in Fig. S1† and cartesian coordinates in Tables S1–S8.† This theoretical study aims to offer valuable insights into the NLO potential of these molecules, paving the way for their practical applications.

### Frontier molecular orbitals (FMOs)

The FMOs analysis is key to understanding chromophores' electronic structure and its impact on NLO characteristics.<sup>25,26</sup> Among FMOs, the HOMO (ability to donate electrons) and LUMO (capability to accept electrons) played significant role in evaluating a substance's dynamic stability and chemical reactivity.<sup>13</sup> Table 1 displays the energies of entitled chromophores calculated at foresaid functional.

The synthesized **BTNC-BNPZ**<sup>14</sup> chromophores exhibit HOMO/LUMO energy levels of  $-5.717/-1.943$ ,  $-5.635/-1.987$ ,  $-5.280/-2.022$  and  $-4.720/-1.936$  eV, respectively. Similarly, the HOMO/LUMO energies of designed derivatives (**BNTP-BNTO**) are  $-5.524/-1.964$ ,  $-5.673/-2.021$ ,  $-5.659/-2.006$  and  $-5.422/2.034$  eV, correspondingly. The higher HOMO energy levels and lower LUMO energy levels in all compounds result in reduced band gaps, significantly improving the charge transfer efficiency in these molecules. Among the **BTNC-BNPZ**,



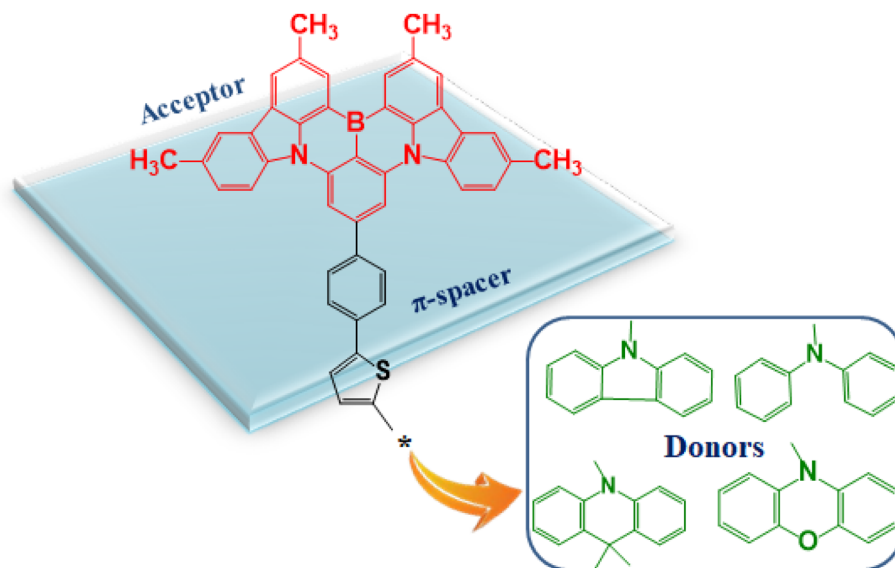


Fig. 1 Schematic representation of the designed chromophores (BNTP–BNTO).

chromophores **BNPZ** exhibit the smallest  $\Delta E$  value of 2.784 eV. This narrow band gap might be due to the efficient electronic interaction between the strong donor moiety (dihydrophenazine) and the acceptor (BNCz core), enhancing internal charge transfer. Similarly, **BNPXZ**, with a smaller energy gap of 3.258 eV compared to **BNAC** 3.648 eV, demonstrates enhanced electronic properties. This is likely due to the combination of the methyl and *p*-tolyl groups in dihydrophenazine moiety, which increases its electron-donating capability relative to the single methyl substitution in phenoxazine. **BTNC** exhibits the highest band gap of 3.774 eV among **BTNC–BNPZ**, possibly due to the less conjugation in the attached carbazole moiety. It might restrict the charge delocalization, in contrast to the more extensive conjugation in dihydrophenazine and phenoxazine. The ascending sequence of  $\Delta E$  of these organic chromophores as follows: **BNPZ** < **BNPXZ** < **BNAC** < **BTNC**. The designed derivative **BNTC** is observed with reduced energy gap of 3.652 eV than **BTNC** chromophore due to the incorporation of 2-phenylthiophene ( $\pi$ -bridge). This  $\pi$ -bridge enhances the conjugation, facilitating better charge delocalization. However, designed compound **BNTA** and chromophore **BNAC** are observed with comparable band gap values. The designed derivatives exhibit an ascending  $\Delta E$  sequence as: **BNTO** < **BNTP** < **BNTC** < **BNTA**.

Fig. 3 illustrates the molecular orbital (MO) surfaces of (**BTNC–BNPZ**) and (**BNTP–BNTO**), depicting the charge transfer from donor moiety towards acceptor units *via*  $\pi$ -spacer. Moreover, Table S9 and Fig. S2† illustrates the energies and counter surfaces of other orbitals (HOMO–1/LUMO+1, HOMO–2/LUMO+2) of studied compounds.

### Global reactivity parameters

The GRDs are determined with the aid of HOMO–LUMO energy values to assess the chemical properties of the molecules. The global softness ( $\sigma$ ),<sup>27</sup> electron affinity (EA),<sup>28</sup> global hardness

( $\eta$ ),<sup>27</sup> global electrophilicity index ( $\omega$ ),<sup>29</sup> chemical potential ( $\mu$ ), ionization potential (IP),<sup>30</sup> and electronegativity ( $X$ )<sup>31</sup> were calculated using eqn (5)–(11).

$$EA = -E_{\text{LUMO}} \quad (5)$$

$$IP = -E_{\text{HOMO}} \quad (6)$$

Koopmans's theorem<sup>32</sup> is used to determine  $\sigma$ ,  $\omega$ ,  $\eta$ ,  $\mu$  and  $X$

$$\eta = \frac{[IP - EA]}{2} \quad (7)$$

$$\sigma = \frac{1}{2\eta} \quad (8)$$

$$X = \frac{[IP + EA]}{2} \quad (9)$$

$$\mu = \frac{E_{\text{HOMO}} + E_{\text{LUMO}}}{2} \quad (10)$$

$$\omega = \frac{\mu^2}{2\eta} \quad (11)$$

The capacity of a chromophore to absorb additional electrical charge from its surroundings is represented by  $\Delta N_{\text{max}}$ <sup>33</sup> which is calculated using eqn (12).

$$\Delta N_{\text{max}} = -\mu/\eta \quad (12)$$

The EA and IP values can be used to quantify the ability of a molecule to accept and donate electrons. The results in Table 2 reveal that aforesaid compounds exhibit a higher IP and a low EA. However, among all the compounds studied, **BTNC** chromophore showed the highest ionization potential, measuring 5.717 eV. The ionization potential decreases in the following



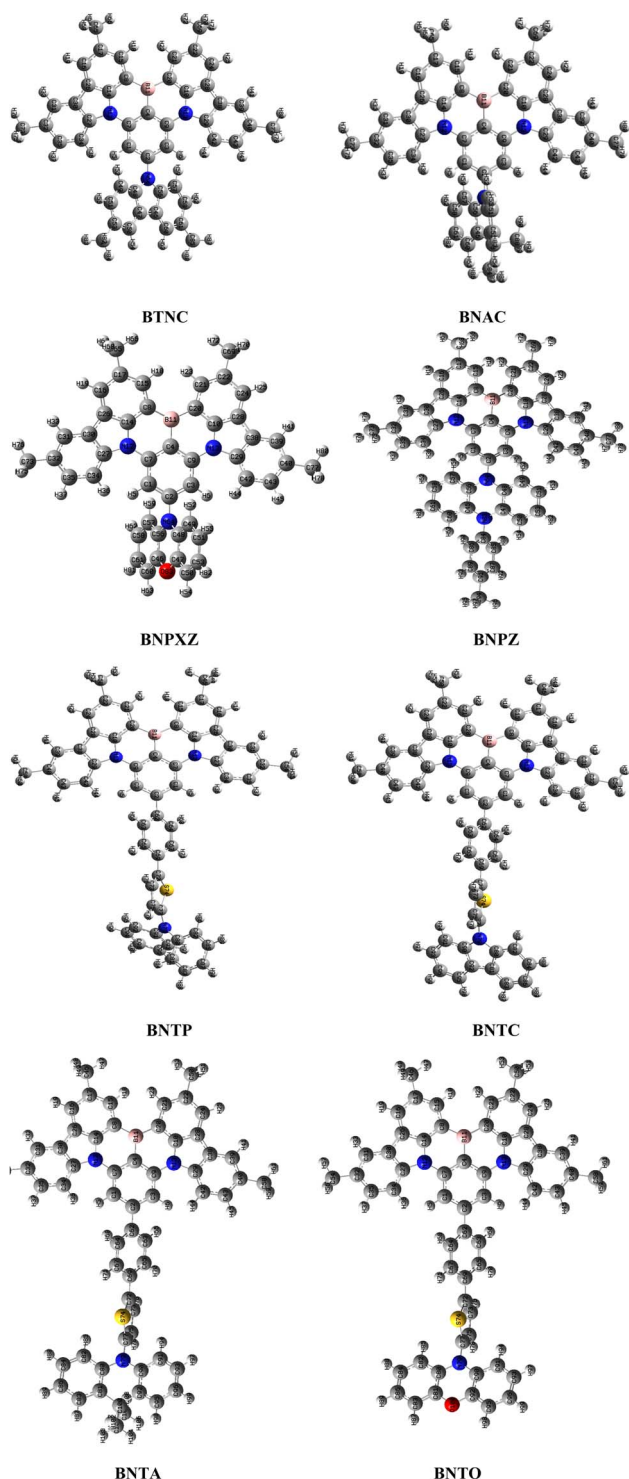


Fig. 2 Optimized structures of studied chromophores.

order: **BTNC** (5.717 eV) > **BNTC** (5.673 eV) > **BNTA** (5.659 eV) > **BNAC** (5.635 eV) > **BNTTP** (5.524 eV) > **BNTD** (5.422 eV) > **BNPXZ** (5.280 eV) > **BNPZ** (4.720 eV). The chemical potential is an important parameter in understanding the tendency of electrons to move away from an equilibrium state. The  $\mu$  values in descending order are: **BNTC** (−3.847 eV) > **BNTA** (−3.833 eV) > **BTNC** (−3.83 eV) > **BNAC** (−3.811 eV) > **BNTTP** (−3.744 eV) >

Table 1 FMOs energies of studied compounds<sup>a</sup>

Chromophores	$E_{\text{HOMO}}$	$E_{\text{LUMO}}$	$\Delta E$
<b>BTNC</b>	−5.717	−1.943	3.774
<b>BNAC</b>	−5.635	−1.987	3.648
<b>BNPXZ</b>	−5.280	−2.022	3.258
<b>BNPZ</b>	−4.720	−1.936	2.784
<b>BNTTP</b>	−5.524	−1.964	3.56
<b>BNTC</b>	−5.673	−2.021	3.652
<b>BNTA</b>	−5.659	−2.006	3.653
<b>BNTD</b>	−5.422	2.034	3.388

<sup>a</sup> Band gap =  $E_{\text{LUMO}} - E_{\text{HOMO}}$ , units in eV.

**BNTD** (−3.728 eV) > **BNPXZ** (−3.651 eV) > **BNPZ** (−3.328 eV). Moreover, **BNTC** and **BNPZ** exhibit the highest and lowest electronegativity values of 3.847 eV and 3.328 eV, respectively. Similarly, global softness and hardness measure the extent of chemical reactivity and are inversely correlated. A molecule with a larger bandgap is deemed harder, more stable, and less reactive, while one with a smaller bandgap is softer, more reactive, and less stable. Among the molecules **BNPZ** shows the highest softness value of 0.359 eV<sup>−1</sup> and the lowest band gap (2.784 eV), making it the most reactive and polarizable compound. Similarly, **BTNC** exhibits the highest hardness value of 1.887 eV and the largest band gap of 3.774 eV, indicating it is the most stable and least reactive compound. The  $\sigma$  values in descending order are: **BNPZ** (0.359 eV<sup>−1</sup>) > **BNPXZ** (0.307 eV<sup>−1</sup>) > **BNTD** (0.295 eV<sup>−1</sup>) > **BNTTP** (0.281 eV<sup>−1</sup>) > **BNAC** (0.274 eV<sup>−1</sup>) = **BNTC** (0.274 eV<sup>−1</sup>) = **BNTA** (0.274 eV<sup>−1</sup>) > **BTNC** (0.265 eV<sup>−1</sup>). Further, **BNPZ** displays the highest  $\Delta N_{\text{max}}$ , with a value of 2.391 eV. In conclusion, the GRP results indicate that **BNPZ** exhibits the highest softness and the lowest band gap (Table 1), demonstrating strongest CT and positioning it as the suitable optoelectronic material for NLO applications.

### Optical properties

UV-Vis calculations for **BTNC**–**BNPZ** and **BNTTP**–**BNTD** were performed in gaseous state at M06/6-311G(d,p) to evaluate charge transfer, contributing configurations, and the nature of electronic transitions.<sup>34,35</sup> Moreover, the impact of various donor moieties and the inclusion of  $\pi$ -spacer on the optical properties of compounds was also examined. The details of absorption maxima ( $\lambda_{\text{max}}$ ), excitation energy ( $\Delta E$ ) and oscillator strength ( $f_{\text{os}}$ ), to transitions are provided in Table 3, while the rest of information is presented in Tables S10–S17.<sup>†</sup>

Fig. 4 shows the simulated absorption spectra of the studied chromophores, ranging from 566.138 to 412.854 nm. The absorption spectra are significantly affected by the donor functionalities in the structure due to the push–pull arrangement in the chromophores. The **BNPZ** chromophore exhibits its maximum absorption peak at 566.138 nm, corresponding to transition energy of 2.190 eV, with 97% contribution from the HOMO to LUMO transition. This peak is likely attributed to the efficient donor moiety, 5-methyl-10-(*p*-tolyl)-5,10-dihydrophenazine. The introduction of donor (10-methyl-10*H*-phenoxazine) in **BNPXZ** has lowered its  $\lambda_{\text{max}}$  to 471.369 nm





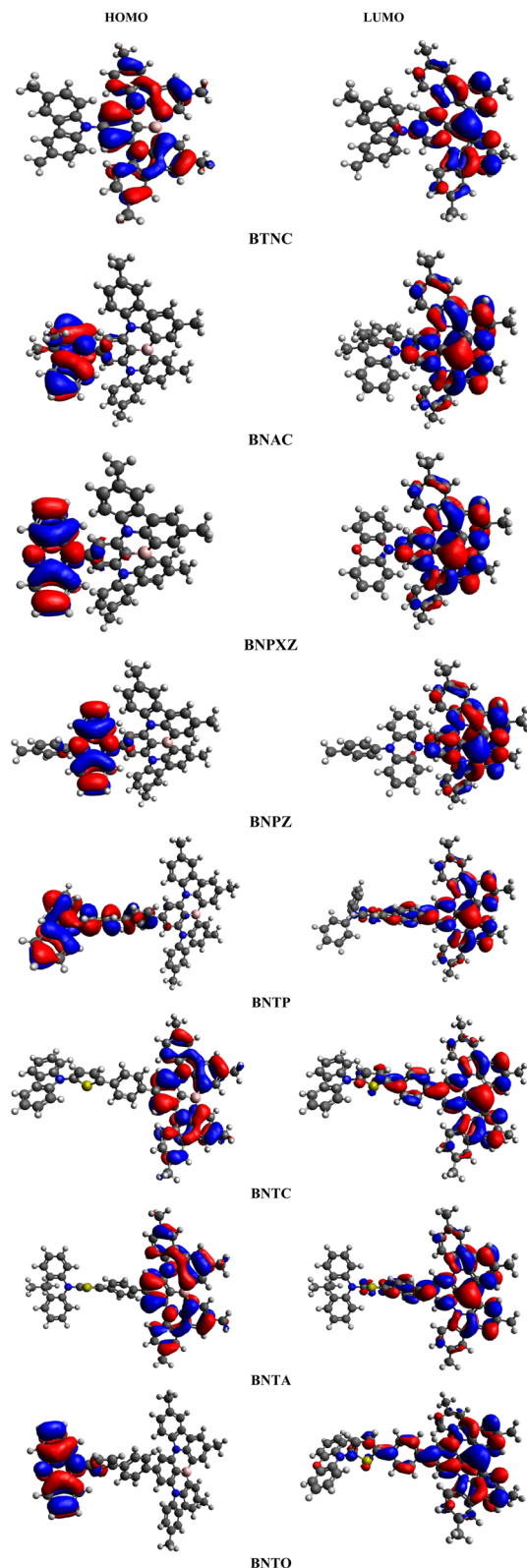


Fig. 3 HOMOs and LUMOs of BTNC–BNPZ and BNTF–BNTD.

associated with transition energy of 2.630 eV. The  $\lambda_{\text{max}}$  further decreases in BNAC and BTNC with the introduction of donors: 9,9,10-trimethyl-9,10-dihydroacridine and 3,6,9-trimethyl-9H-

carbazole, resulting in absorption peaks at 418.286 and 412.854 nm, respectively. The compounds are ordered in decreasing absorption peak as follows: **BNPZ** > **BNPXZ** > **BNAC** > **BTNC**.

Among the designed compounds, **BNTD** featuring a dihydrophenazine donor showed highest absorption at 426.326 nm, the lowest transition energy of 2.908 eV, and 96% H–1  $\rightarrow$  L contribution. Comparing **BTNC** and **BNTC**, both with dihydroacridine donors, **BNTC** showed a greater red shift at 425.405 nm due to the added  $\pi$ -bridge, which enhances the charge transfer rate. Similarly, by incorporating a phenylthiophene linker in **BNTA**, compared to **BNAC**, both containing phenoxazine donor, **BNTA** showed with higher absorption at 425.434 nm. Overall, the  $\lambda_{\text{max}}$  of designed compounds are found to follow this increasing order: **BNTD** > **BNTF** > **BNTA** > **BNTC**. Hence, all the explored chromophores, particularly **BNPZ** and **BNTD**, show promising potential as high-performance optoelectronic materials, owing to their good absorption and charge transfer properties.

### Density of states analysis

The density of states analysis confirms the findings shown by FMO study and provides insight into the electronic distribution from HOMO to LUMO.<sup>36,37</sup> In DOS graphs, the HOMO corresponds to the valence band, reflecting right side, while the conduction band (LUMO) is represented by left side.<sup>38</sup> The partition between the conduction and valence bands represents the energy band gap. The DOS maps for **BTNC**–**BNPZ** and **BNTF**–**BNTD** were illustrated in Fig. 5. It reveals the contribution of each molecular fragment to the charge transfer. To calculate the density of states, chromophores **BTNC**–**BNPZ** were separated into two fragments: the donor and the acceptor (BNCz core), whereas the derivatives: **BNTF**–**BNTD** were partitioned into three segments: donor,  $\pi$ -spacer (2-phenylthiophene), and acceptor (BNCz core). In DOS maps, red, green, and blue peaks illustrated the donor,  $\pi$ -spacer, and acceptor, respectively, with the black band indicating the molecule's overall electronic contribution, as shown in Fig. 5.

Table 4 shows that donors contribute 2.1, 0.9, 1.4, and 1.2 to the LUMO, and 0.4, 95.7, 95.8, and 97.4 to the HOMO for **BTNC**–**BNPZ**, respectively. While the acceptor contributes 97.9, 99.1, 98.6, and 98.8 to the LUMO, with its HOMO contributions being 99.6, 4.3, 4.2, and 2.6% for **BTNC**–**BNPZ**, respectively. For **BNTF**–**BNTD** series the acceptor contributes 2.4, 99.8, 99.8, 0.0 to HOMO and 86.1, 84.8, 85.3 and 82.8 to LUMO, respectively (Table 5). Moreover, the charge contribution of the donor to HOMO and LUMO is 55.8, 0.0, 0.0 and 95.9, and 50.1% and 0.5, 0.2, 0.2, 0.2, and 0.2%, respectively. Similarly,  $\pi$ -spacer account to HOMO is 41.8, 0.2, 0.2, and 4.1% while their participation to LUMO is 13.4, 15.0, 14.5 and 17.0% for **BNTF**–**BNTD**, respectively.

### Transition density matrix (TDM) investigation

The TDM study serves as an effective method for evaluating transmission of electronic density between two quantum states.<sup>39,40</sup> In molecular systems, TDM analysis generates 3D



Table 2 The GRPs of BTNC–BNPZ and BNTP–BNT0<sup>a</sup>

Chromophores	IP	EA	<i>X</i>	$\eta$	$\mu$	$\omega$	$\sigma$	$\Delta N_{\max}$
BTNC	5.717	1.943	3.83	1.887	−3.83	3.887	0.265	2.029
BNAC	5.635	1.987	3.811	1.824	−3.811	3.981	0.274	2.089
BNPXZ	5.280	2.022	3.651	1.629	−3.651	4.092	0.307	2.241
BNPZ	4.720	1.936	3.328	1.392	−3.328	3.978	0.359	2.391
BNTP	5.524	1.964	3.744	1.78	−3.744	3.938	0.281	2.103
BNTC	5.673	2.021	3.847	1.826	−3.847	4.053	0.274	2.107
BNTA	5.659	2.006	3.833	1.827	−3.833	4.021	0.274	2.099
BNT0	5.422	2.034	3.728	1.694	−3.728	4.102	0.295	2.201

<sup>a</sup> Global softness ( $\sigma$ ) eV<sup>−1</sup>, all other units in eV.Table 3 Wavelength ( $\lambda$ ), excitation energy (*E*), oscillator strength ( $f_{os}$ ) and nature of molecular orbital contributions of compounds (BTNC–BNPZ) and (BNTP–BNT0) in gaseous phase<sup>a</sup>

Compounds	DFT $\lambda$ (nm)	<i>E</i> (eV)	$f_{os}$	MO contributions
BTNC	412.854	3.003	0.378	H → L (97%)
BNAC	418.286	2.964	0.375	H−1 → L (90%)
BNPXZ	471.369	2.630	0.039	H → L (96%)
BNPZ	566.138	2.190	0.026	H → L (97%)
BNTP	425.565	2.913	0.365	H−1 → L (97%)
BNTC	425.405	2.915	0.365	H → L (97%)
BNTA	425.434	2.914	0.363	H → L (97%)
BNT0	426.326	2.908	0.358	H−1 → L (96%)

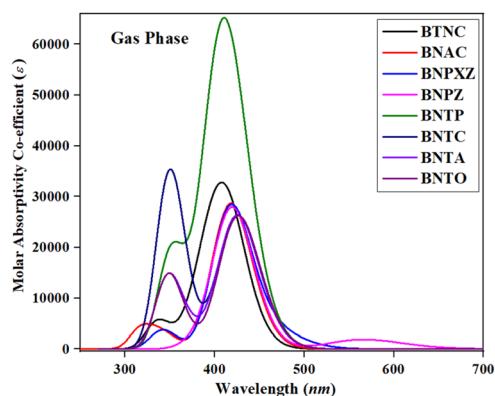
<sup>a</sup> MO = molecular orbital, H=HOMO, L = LUMO,  $f_{os}$  = oscillator strength, DFT = density functional theory.

Fig. 4 Simulated absorption spectra in gas phase of examined chromophores.

heat maps that depict charge carrier distribution, and allow the observation of their coherence and delocalization.<sup>41,42</sup> Transition density matrix maps of the studied compounds have been calculated in gaseous state and are presented in Fig. 6. It aids in examining the donor–acceptor interaction in the excited state and the localization of electron holes.<sup>43</sup> The H atoms are omitted in this study due to their negligible contribution to the transition. To generate TDM maps, the BTNC–BNPZ chromophores were divided into two components: “A” and “D”, while the BNTP–BNT0 chromophores were split into three distinct

parts: “D”,  $\pi$ -spacer, and “A”. The  $\pi$ -spacer functions as a pathway for CT by enabling relations between the donor and acceptor components. The TDM diagrams show that in BTNC–BNPZ and BNTP–BNT0 molecules, an efficient diagonal transfer of charge mobility from donor to the acceptor through the  $\pi$ -spacer. The FMOs study (Fig. 3) reveals that charge transfer occurs significantly towards “A” from “D” through linker, which results in support the TDM heat maps. According to Fig. 6, diagonal charge coherence is observed in BTNC and BNAC from donor to acceptor portions whereas in BNAC and BNPXZ non-diagonal coherence is observed. In designed chromophores (BNTP–BNT0) efficient charge coherence is noted from “D” to “A” regions *via* the  $\pi$ -spacer.

### Exciton binding energy ( $E_b$ )

The  $E_b$  is a crucial parameter for evaluating the optoelectronic properties of the studied compounds.<sup>44</sup> A lower binding energy leads to enhanced charge mobility, resulting in a stronger NLO response. The  $E_b$  of BTNC–BNPZ and BNTP–BNT0 were determined by subtracting the first excitation energies ( $E_{opt}$ ) from the band gap ( $E_{gap}$ ) using eqn (13).

$$E_b = E_{H-L} - E_{opt} \quad (13)$$

The values of  $E_b$  for BTNC–BNPZ and BNTP–BNT0 are computed to be 0.771, 0.684, 0.628, 0.594, 0.647, 0.737, 0.739 eV, respectively (Table 6). Among all the examined chromophores, BNPZ showed the lowest exciton binding energy of 0.594 eV, suggesting superior exciton separation and enhanced charge density potential. To list the compounds in decreasing order of binding energy ( $E_b$ ) is: BTNC > BNTA > BNTC > BNAC > BNTP > BNPXZ > BNPZ. The least values of  $E_b$  illustrated the good CT in entitled chromophores which supported the greater polarity in them resulting good NLO response.

### Natural population analysis (NPA)

The calculation of atomic charges, that reveal the charge distribution across different atoms of a molecule, is essential for predicting changes in bond lengths. These charges are crucial in influencing the dipole moment, electronic structure, molecular polarizability, and other key properties of molecular systems.<sup>45</sup>



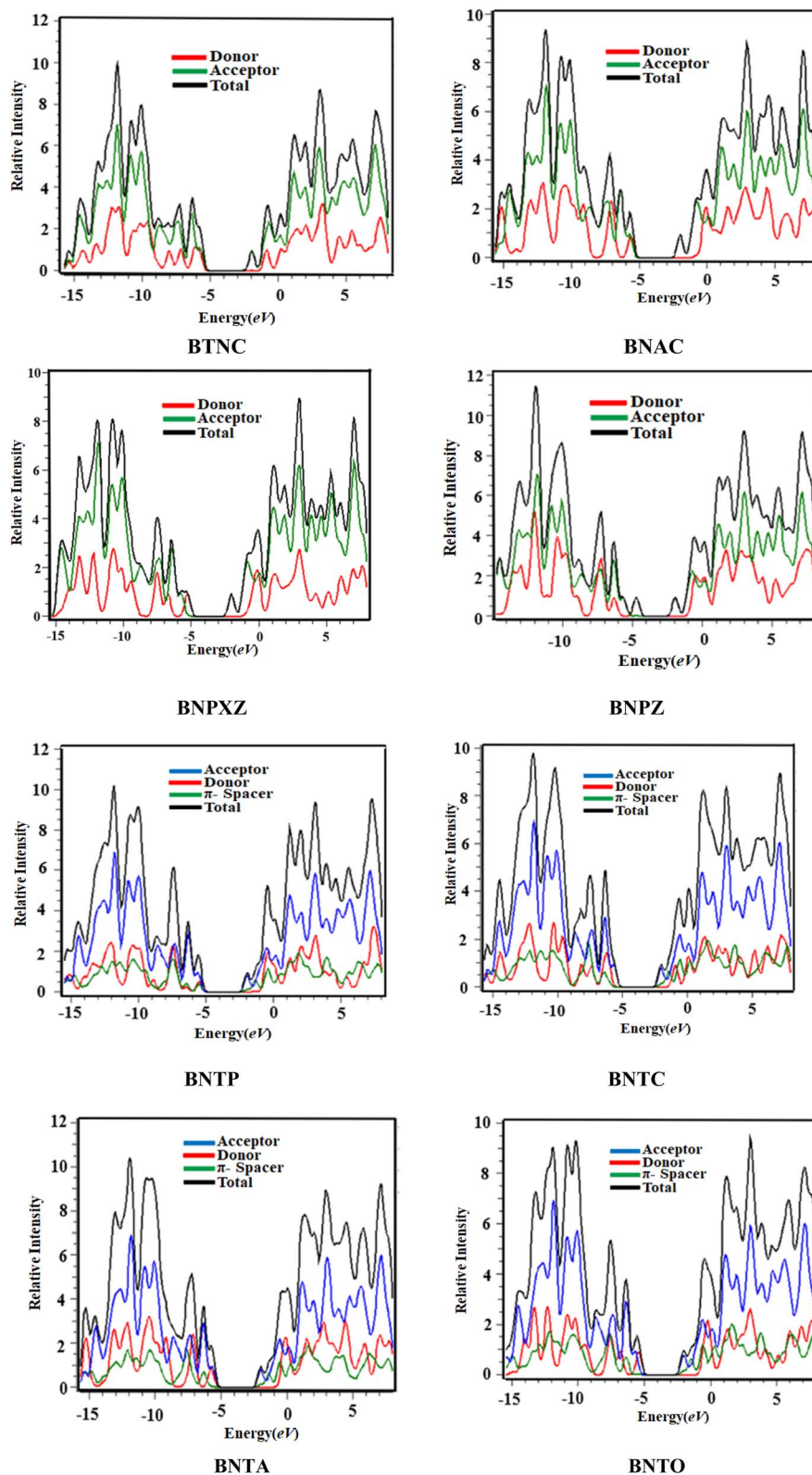


Fig. 5 The DOS plots of the examined chromophores.

Fig. S3† presents the NPA analysis results; illustrate the natural charge distribution in compounds **BTNC**–**BNPZ** and **BNTP**–**BNTO**. The distribution of electrical charges on

individual atoms significantly influences the arrangement of molecules and their bonding potential. The natural charge analysis indicates that electronegative elements (B, N, O, S)





**Table 4** Percentages of acceptor, donor for LUMO and HOMO OF BTNC–BNPZ

Compounds	LUMO		HOMO	
	Acceptor	Donor	Acceptor	Donor
<b>BTNC</b>	97.9	2.1	99.6	0.4
<b>BNAC</b>	99.1	0.9	4.3	95.7
<b>BNPXZ</b>	98.6	1.4	4.2	95.8
<b>BNPZ</b>	98.8	1.2	2.6	97.4

**Table 5** Percentages of acceptor, donor and  $\pi$ -spacer for LUMO and HOMO of BNTP–BNT0

Compounds	LUMO			HOMO		
	Acceptor	$\pi$ -spacer	Donor	Acceptor	$\pi$ -spacer	Donor
<b>BNTP</b>	86.1	13.4	0.5	2.4	41.8	55.8
<b>BNTC</b>	84.8	15.0	0.2	99.8	0.2	0.0
<b>BNTA</b>	85.3	14.5	0.2	99.8	0.2	0.0
<b>BNT0</b>	82.8	17.0	0.2	0.0	4.1	95.9

induce uneven electron density redistribution across the heteroatomic rings. Additionally, negative charges on carbon atoms result in hydrogen atoms acquiring positive charges. The NPA graphs reveal that all H, S, and Br atoms carry positive charges, but N and O contain negative charges. Moreover, certain carbon atoms carry a positive charge, while others are assigned a negative charge. The significant negative charge on carbon atoms results from their resonance interaction with adjacent N and O atoms. 11B in **BTNC–BNPZ** are observed with significant positive charges while 64 N with higher negative charges. Similarly, 11B and 79N display notably positive and negative charges in **BNTP–BNT0**, respectively. This might be due to the presence of highly negative and positive atoms around them, respectively.

### Natural bond orbital (NBO) analysis

NBO analysis is the most accurate method for interpreting electrophilic, nucleophilic and hyper-conjugative interactions, orbitals interactions, and the nature of electronic transitions.<sup>46,47</sup> Furthermore, NBO study facilitates the analysis of electron density transfer between unoccupied (A) and occupied (D) molecular orbitals in D– $\pi$ –A framework.<sup>17,46,48</sup> The second-order perturbation method is utilized to assess the reactions that entail delocalization.<sup>47</sup> To compute the stabilization energy  $E^{(2)}$ , for each donor ( $i$ ) to acceptor ( $j$ ) interaction which results in  $i \rightarrow j$  delocalization, eqn (14) is used.

$$E^{(2)} = \Delta E_{ij} = q_i \frac{(F_{ij})^2}{(E_j - E_i)} \quad (14)$$

The D orbital occupancy is symbolized by  $q_i$ ; the diagonal and off-diagonal NBO Fock matrix elements are signified by  $E_j - E_i$  and  $F_{ij}$ , respectively.<sup>49</sup> Orbital overlap leads to various

hyperconjugative interactions:  $\sigma \rightarrow \sigma^*$ ,  $\pi \rightarrow \pi^*$ ,  $LP \rightarrow \sigma^*$ , and  $LP \rightarrow \pi^*$ . The  $\pi$ -conjugation in investigated compounds featuring D–A and D– $\pi$ –A framework facilitates  $\pi \rightarrow \pi^*$  transitions, making them highly efficient NLO materials. Weak  $\sigma \rightarrow \sigma^*$  transitions are also observed due to less interactions between donor and acceptor moieties. Table 7 highlights the key transition values for (**BTNC–BNPZ**) and (**BNTP–BNT0**), while comprehensive data is provided in Tables S18–S25.<sup>†</sup>

Table 7 shows that in compound **BTNC**, the most significant  $\pi \rightarrow \pi^*$  interaction involves  $\pi(C1-C7)$  donating to  $\pi^*(C2-C3)$  with  $E^{(2)}$  of 28.95 kcal mol<sup>−1</sup>, while the weakest occurs between  $\pi(C1-C7)$  and its own  $\pi^*$  orbital, with an energy of 0.82 kcal mol<sup>−1</sup>. Among  $\sigma \rightarrow \sigma^*$  transitions, the strongest is from  $\sigma(C34-C35)$  to  $\sigma^*(N12-C27)$  at  $E^{(2)}$  of 6.81 kcal mol<sup>−1</sup>, and the weakest is at 0.97 kcal mol<sup>−1</sup> for  $\sigma(N12-C27) \rightarrow \sigma^*(C34-C35)$  transition. The  $LP \rightarrow \pi^*$  interaction is dominated by  $LP1(N12)$  donating to  $\pi^*(C1-C7)$ , contributing 41.16 kcal mol<sup>−1</sup>. Meanwhile, for  $LP \rightarrow \sigma^*$  transition, smallest  $E^{(2)}$  for  $LP1(N64) \rightarrow \sigma^*(C1-C2)$  is noted at 3.5 kcal mol<sup>−1</sup>. In **BNAC**, the most prominent  $\pi \rightarrow \pi^*$  donation comes from  $\pi(C1-C7)$  to  $\pi^*(C2-C3)$ , exhibiting an  $E^{(2)}$  of 28.89 kcal mol<sup>−1</sup>, whereas the weakest  $\pi$  interaction is calculated at  $E^{(2)} = 0.83$  kcal mol<sup>−1</sup> from  $\pi(C10-C20)$  to  $\pi^*(C10-C20)$ . The strongest  $\sigma \rightarrow \sigma^*$  interaction,  $\sigma(C34-C35) \rightarrow \sigma^*(N12-C27)$ , occurs at 6.79 kcal mol<sup>−1</sup> stabilization energy, with the weakest being  $\sigma(C16-H19) \rightarrow \sigma^*(C16-C17)$  at 0.99 kcal mol<sup>−1</sup>. The leading  $LP \rightarrow \pi^*$  contribution is 40.99 kcal mol<sup>−1</sup> for  $LP1(N12) \rightarrow \pi^*(C1-C7)$ , while  $LP1(N64) \rightarrow \sigma^*(C1-C2)$  registers the smallest  $LP \rightarrow \sigma^*$  value of 6.76 kcal mol<sup>−1</sup>. For compound **BNPXZ**, the highest  $\pi \rightarrow \pi^*$  interaction involves  $\pi(C1-C7)$  donating to  $\pi^*(C2-C3)$ , with an energy of 29.05 kcal mol<sup>−1</sup>, while the lowest is 0.65 kcal mol<sup>−1</sup> for  $\pi(C1-C7) \rightarrow \pi^*(C1-C7)$ . The  $\sigma \rightarrow \sigma^*$  donation from  $\sigma(C42-C43)$  to  $\sigma^*(N13-C29)$  is the strongest at 6.79 kcal mol<sup>−1</sup>, and the weakest, 0.51 kcal mol<sup>−1</sup>, is from  $\sigma(C39-C40)$  to  $\sigma^*(C77-H78)$ .  $LP \rightarrow \pi^*$  interactions are led by  $LP2(O83) \rightarrow \pi^*(C46-C60)$  with an energy of 24.72 kcal mol<sup>−1</sup>, and the smallest  $LP \rightarrow \sigma^*$  interaction comes from  $LP1(O83) \rightarrow \sigma^*(C47-C48)$  at 6.72 kcal mol<sup>−1</sup>. In **BNPZ**, the most dominant  $\pi \rightarrow \pi^*$  transition occurs between  $\pi(C1-C7)$  and  $\pi^*(C2-C3)$ , showing an energy of 29.06 kcal mol<sup>−1</sup>, while the weakest  $\pi \rightarrow \pi^*$  interaction at 0.82 kcal mol<sup>−1</sup> involves  $\pi(C10-C20) \rightarrow \pi^*(C10-C20)$ . The  $\sigma \rightarrow \sigma^*$  transition with the highest energy, 6.76 kcal mol<sup>−1</sup>, is  $\sigma(C34-C35) \rightarrow \sigma^*(N12-C27)$ , whereas the lowest is 0.97 kcal mol<sup>−1</sup> for  $\sigma(N12-C27) \rightarrow \sigma^*(C34-C35)$ . The  $LP \rightarrow \pi^*$  interaction of  $LP1(N12) \rightarrow \pi^*(C1-C7)$  dominates with an energy of 40.48 kcal mol<sup>−1</sup>, and the weakest  $LP \rightarrow \sigma^*$  transition is  $LP1(N83) \rightarrow \sigma^*(C84-C86)$  at 6.54 kcal mol<sup>−1</sup>. Moving to the series of designed compounds for **BNTP**, the highest  $\pi \rightarrow \pi^*$  transition occurs at 28.1 kcal mol<sup>−1</sup> for  $\pi(C1-C7) \rightarrow \pi^*(C2-C3)$ , and the lowest is at 1.68 kcal mol<sup>−1</sup> stabilization energy for  $\pi(C4-C9) \rightarrow \pi^*(C4-C9)$ . The highest  $\sigma \rightarrow \sigma^*$  transition is at 6.9 kcal mol<sup>−1</sup> energy for  $\sigma(C73-C75) \rightarrow \sigma^*(C77-N79)$ , and the lowest is at 0.99 kcal mol<sup>−1</sup> for  $\sigma(C24-H25) \rightarrow \sigma^*(C22-C24)$ . The highest  $LP \rightarrow \pi^*$  transition occurs at 24.27 kcal mol<sup>−1</sup> energy, observed for  $LP2(S74) \rightarrow \pi^*(C75-C77)$ , while the lowest is at 10.21 kcal mol<sup>−1</sup> stabilization energy for  $LP1(N79) \rightarrow \sigma^*(S74-C77)$ . For compound **BNTC**, the highest  $\pi \rightarrow \pi^*$





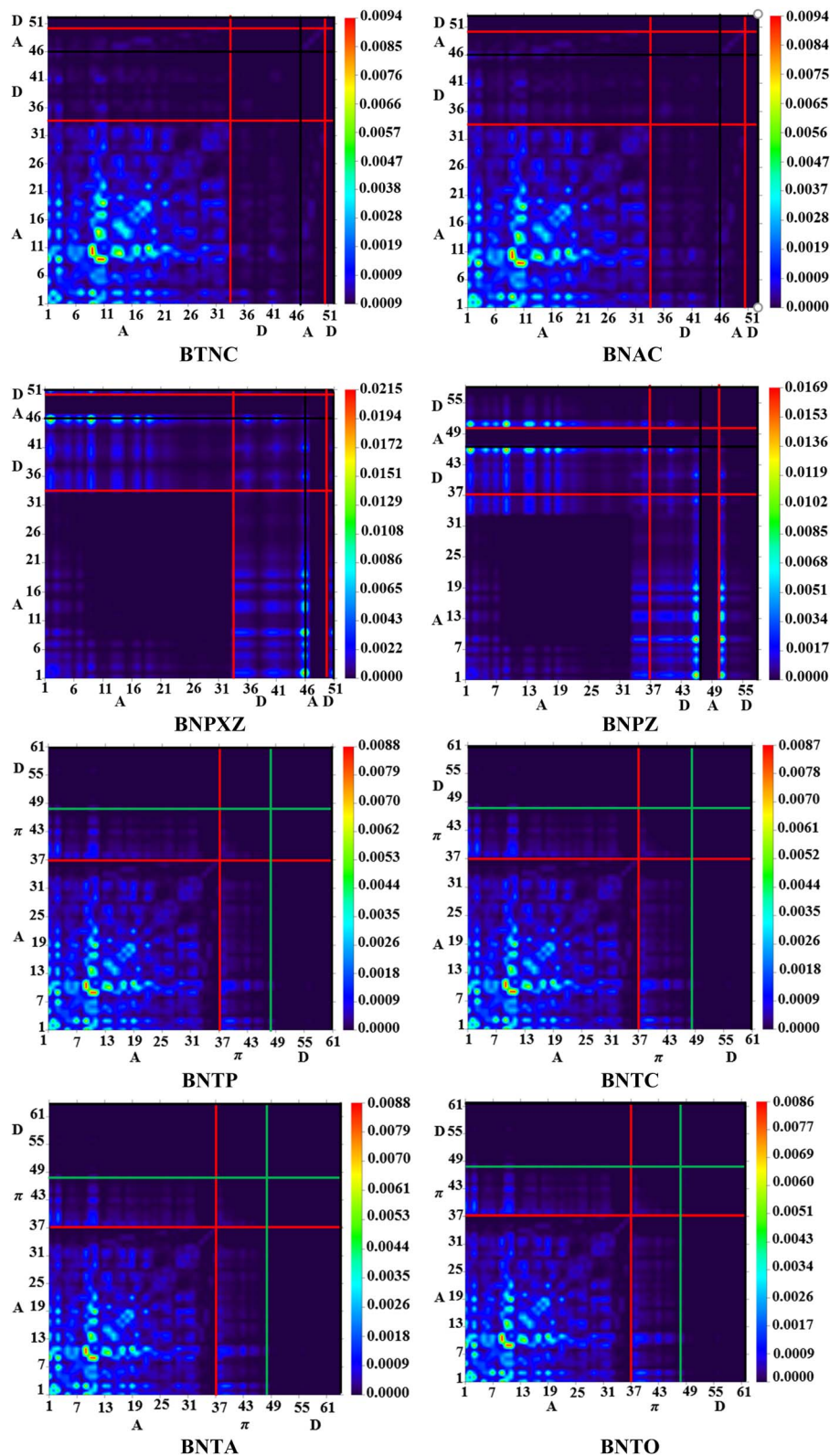


Fig. 6 TDM in the examined compounds (BTNC–BNPZ) and (BNTD–BNTD).

transition is observed at 28.31 kcal mol<sup>−1</sup> for  $\pi(\text{C1–C7}) \rightarrow \pi^*(\text{C2–C3})$ , with the lowest at 0.83 kcal mol<sup>−1</sup> energy for  $\pi(\text{C10–C20}) \rightarrow \pi^*(\text{C10–C20})$ . The highest  $\sigma \rightarrow \sigma^*$  transition energy is

6.91 kcal mol<sup>−1</sup> for  $\sigma(\text{C73–C75}) \rightarrow \sigma^*(\text{C77–N79})$ , and the lowest is 1.98 kcal mol<sup>−1</sup> for  $\sigma(\text{C9–N13}) \rightarrow \sigma^*(\text{C3–C9})$ . The highest LP  $\rightarrow \pi^*$  transition energy is 25.02 kcal mol<sup>−1</sup> for LP2(S74)  $\rightarrow$



Table 6 Exciton cohesion energies of (BTNC–BNPZ) and (BNTP–BNTQ)<sup>a</sup>

Compounds	$E_{H-L}$	$E_{opt}$	$E_b$
<b>BTNC</b>	3.774	3.003	0.771
<b>BNAC</b>	3.648	2.964	0.684
<b>BNPXZ</b>	3.258	2.630	0.628
<b>BNPZ</b>	2.784	2.190	0.594
<b>BNTP</b>	3.56	2.913	0.647
<b>BNTC</b>	3.652	2.915	0.737
<b>BNTA</b>	3.653	2.914	0.739

<sup>a</sup> Units in eV.

$\pi^*(C72-C73)$ , and the lowest is 13.43 kcal mol<sup>-1</sup> for LP1(N79)  $\rightarrow \sigma^*(S74-C77)$ . For compound **BNTA**, the maximum  $\pi \rightarrow \pi^*$  transition occur at stabilization energy of 28.22 kcal mol<sup>-1</sup> for  $\pi(C1-C7) \rightarrow \pi^*(C2-C3)$ , while the minimum value of stabilization energy is 0.83 kcal mol<sup>-1</sup> for  $\pi(C10-C20) \rightarrow \pi^*(C10-C20)$ . The highest  $\sigma \rightarrow \sigma^*$  transition occurs at 6.88 kcal mol<sup>-1</sup> for  $\sigma(C73-C75) \rightarrow \sigma^*(C77-N79)$ , and the lowest at 0.99 kcal mol<sup>-1</sup> for  $\sigma(C16-H19) \rightarrow \sigma^*(C16-C17)$ . The maximum LP  $\rightarrow \pi^*$  transition is noted at 25.04 kcal mol<sup>-1</sup> for LP2(S74)  $\rightarrow \pi^*(C72-C73)$ , and the minimum is found at 16.26 kcal mol<sup>-1</sup> for LP1(N79)  $\rightarrow \sigma^*(S74-C77)$ . For compound **BNTQ**, the highest  $\pi \rightarrow \pi^*$  transition energy is 28.21 kcal mol<sup>-1</sup> for  $\pi(C1-C7) \rightarrow \pi^*(C2-C3)$ , with the lowest value at 0.83 kcal mol<sup>-1</sup> for  $\pi(C10-C20) \rightarrow \pi^*(C10-C20)$ . The highest  $\sigma \rightarrow \sigma^*$  transition is 7.04 kcal mol<sup>-1</sup> for  $\sigma(C73-C75) \rightarrow \sigma^*(C77-N79)$ , and the lowest is 0.99 kcal mol<sup>-1</sup> for  $\sigma(C24-H25) \rightarrow \sigma^*(C22-C24)$ . The highest LP  $\rightarrow \pi^*$  transition energy is 25.26 kcal mol<sup>-1</sup> for LP2(S74)  $\rightarrow \pi^*(C72-C73)$ , while the lowest is 15.89 kcal mol<sup>-1</sup> for LP1(N79)  $\rightarrow \sigma^*(S74-C77)$ . Hence, the NBO analysis of the aforementioned molecules indicates that strong intramolecular charge transfer and extensive hyperconjugation significantly contribute to their stabilization and impart remarkable NLO properties.

### Non-linear optical (NLO) study

Hyperpolarizability and intramolecular charge transfer (ICT) elucidate the connection between molecular structure and nonlinearity.<sup>50,51</sup> High molecular polarizability, significant dipole moment, and hyperpolarizability values collectively enhance NLO performance. The ability of an electric field to distort the electronic distribution within a molecule is referred to as linear polarizability ( $\langle\alpha\rangle$ ). Hyperpolarizability ( $\beta$ ,  $\gamma$ ) refers to the atomic and molecular nonlinearity underlying various nonlinear optical phenomena.<sup>52</sup> The values of first-order hyperpolarizability ( $\beta_{tot}$ ), second-order hyperpolarizability ( $\gamma_{tot}$ ), linear polarizability ( $\langle\alpha\rangle$ ), and dipole moment ( $\mu_{tot}$ ), along with their respective tensors for **BTNC–BNPZ** and **BNTP–BNTQ**, are provided in Tables S26–S29† and 8.

The  $\mu$  plays a crucial role in evaluating the polarizability of organic chromophores. It is determined by the product of the magnitude of charges and the distance separating them. Table S26† displays the calculated dipole moment values along with the three-dimensional tensor components in the  $x$ ,  $y$ , and  $z$

Table 7 Computed NBO analysis for studied chromophores

Compounds	Donor (i)	Type	Acceptor (j)	Type	$E^{(2)}$ [kcal mol <sup>-1</sup> ]
<b>BTNC</b>	C1–C7	$\pi$	C2–C3	$\pi^*$	28.95
	C1–C7	$\pi$	C1–C7	$\pi^*$	0.82
	C34–C35	$\sigma$	N12–C27	$\sigma^*$	6.81
	N12–C27	$\sigma$	C34–C35	$\sigma^*$	0.97
	N12	LP1	C1–C7	$\pi^*$	41.16
<b>BNAC</b>	N64	LP1	C1–C2	$\sigma^*$	3.5
	C1–C7	$\pi$	C2–C3	$\pi^*$	28.89
	C10–C20	$\pi$	C10–C20	$\pi^*$	0.83
	C34–C35	$\sigma$	N12–C27	$\sigma^*$	6.79
	C16–H19	$\sigma$	C16–C17	$\sigma^*$	0.99
<b>BNPXZ</b>	N12	LP1	C1–C7	$\pi^*$	40.99
	N64	LP1	C1–C2	$\sigma^*$	6.76
	C1–C7	$\pi$	C2–C3	$\pi^*$	29.05
	C1–C7	$\pi$	C1–C7	$\pi^*$	0.65
	C42–C43	$\sigma$	N13–C29	$\sigma^*$	6.79
<b>BNPZ</b>	C39–C40	$\sigma$	C77–H78	$\sigma^*$	0.51
	O83	LP2	C46–C60	$\pi^*$	24.72
	O83	LP1	C47–C48	$\sigma^*$	6.72
	C1–C7	$\pi$	C2–C3	$\pi^*$	29.06
	C10–C20	$\pi$	C10–C20	$\pi^*$	0.82
<b>BNTP</b>	C34–C35	$\sigma$	N12–C27	$\sigma^*$	6.76
	N12–C27	$\sigma$	C34–C35	$\sigma^*$	0.97
	N12	LP1	C1–C7	$\pi^*$	40.48
	N83	LP1	C84–C86	$\sigma^*$	6.54
	C1–C7	$\pi$	C2–C3	$\pi^*$	28.1
<b>BNTC</b>	C4–C9	$\pi$	C4–C9	$\pi^*$	1.68
	C73–C75	$\sigma$	C77–N79	$\sigma^*$	6.9
	C24–H25	$\sigma$	C22–C24	$\sigma^*$	0.99
	S74	LP2	C75–C77	$\pi^*$	24.27
	N79	LP1	C74–C77	$\sigma^*$	10.31
<b>BNTA</b>	C1–C7	$\pi$	C2–C3	$\pi^*$	28.31
	C10–C20	$\pi$	C10–C20	$\pi^*$	0.83
	C73–C75	$\sigma$	C77–N79	$\sigma^*$	6.91
	C9–N13	$\sigma$	C3–C9	$\sigma^*$	1.98
	S74	LP2	C72–C73	$\pi^*$	25.02
<b>BNTQ</b>	N79	LP1	C74–C77	$\sigma^*$	13.43
	C1–C7	$\pi$	C2–C3	$\pi^*$	28.22
	C10–C20	$\pi$	C10–C20	$\pi^*$	0.83
	C73–C75	$\sigma$	C77–N79	$\sigma^*$	6.88
	C16–H19	$\sigma$	C16–C17	$\sigma^*$	0.99
<b>BNTQ</b>	S74	LP2	C72–C73	$\pi^*$	25.04
	N79	LP1	C74–C77	$\sigma^*$	16.26
	C1–C7	$\pi$	C2–C3	$\pi^*$	28.21
	C10–C20	$\pi$	C10–C20	$\pi^*$	0.83
	C73–C75	$\sigma$	C77–N79	$\sigma^*$	7.04
<b>BNTQ</b>	C24–H25	$\sigma$	C22–C24	$\sigma^*$	0.99
	S74	LP2	C72–C73	$\pi^*$	25.26
	N97	LP1	S74–C77	$\sigma^*$	15.89

directions. The  $\mu_{tot}$  of the compounds in decreasing order are as follows in Debye: **BNPXZ** (2.046) > **BNTQ** (1.952) > **BNTC** > (1.564) > **BTNC** (1.308) > **BNPZ** (1.191) > **BNAC** (1.110) > **BNTP** (1.000) = **BNTA** (1.000). Among all the compounds, **BNPXZ** exhibits the highest  $\mu$  value (2.046 D), indicating the strongest polarity, while **BNTA** and **BNTP** both have the lowest  $\mu$  (1.000 D), signifying their least polarity. For the studied compounds **BTNC**, **BNAC**, **BNPXZ**, **BNPZ**, **BNTP**, **BNTC**, **BNTA**, and **BNTQ**, the dominant tensor lies along the  $\mu_x$  axis, with values of  $-1.3084$ ,  $-1.0776$ ,  $0.0307$ ,  $-1.1899$ ,  $0.9027$ ,  $-1.3190$ ,  $0.3779$ ,



**Table 8** Computed  $\mu_{\text{tot}}$ ,  $\langle\alpha\rangle$ ,  $\beta_{\text{tot}}$ , and  $\gamma_{\text{tot}}$  for the synthesized molecules<sup>a</sup>

Compounds	$\mu_{\text{tot}}$	$\langle\alpha\rangle \times 10^{-23}$	$\beta_{\text{tot}} \times 10^{-30}$	$\gamma_{\text{tot}} \times 10^{-35}$
<b>BTNC</b>	1.308	9.68	19.0	24.0
<b>BNAC</b>	1.110	9.55	7.11	16.5
<b>BNPXZ</b>	2.046	9.16	6.42	21.4
<b>BNPZ</b>	1.191	10.5	18.5	29.5
<b>BNTF</b>	1.000	11.9	74.0	81.1
<b>BNTC</b>	1.564	11.7	17.0	46.2
<b>BNTA</b>	1.000	12.2	18.0	47.7
<b>BNTD</b>	1.952	11.7	15.0	46.9

<sup>a</sup> Units in esu.  $\mu_{\text{tot}}$  in Debye.

and 1.6581 D, respectively, indicating it as the primary contribution of polarity. In contrast, **BNPXZ** shows its highest dipole moment along the  $\mu_y$  axis (2.0474 D). The facts from Table S27<sup>†</sup> reveals that all the studied chromophores exhibit higher linear polarizability along the  $\alpha_{xx}$  tensor except **BTNC** and **BNAC**, where  $\alpha_{yy}$  dominate. The evaluation of average polarizability indicates that **BNTA** exhibits the highest average polarizability ( $\langle\alpha\rangle = 12.2 \times 10^{-23}$  esu), with tensor components  $\alpha_{xx} = 1.67 \times 10^{-22}$ ,  $\alpha_{yy} = 1.42 \times 10^{-22}$ , and  $\alpha_{zz} = 5.57 \times 10^{-23}$  esu along the  $x$ ,  $y$ , and  $z$  axes, respectively. Designing new D- $\pi$ -A frameworks enable CT between electron accepting and donating parts, reducing the band gap and enhancing first hyperpolarizability ( $\beta_{\text{tot}}$ ). The calculated first hyperpolarizability values of entitled compounds, along with their respective tensor components, are presented in Table S29.<sup>†</sup> The investigated chromophores show remarkable  $\beta_{\text{tot}}$  values ranging from  $6.42 \times 10^{-30}$  to  $74.20 \times 10^{-30}$  esu, demonstrating strong nonlinear optical responses. Among the designed derivatives, **BNTF** exhibits the highest  $\beta_{\text{tot}}$  value ( $74.0 \times 10^{-30}$  esu), likely due to strong electronic communication within its push-pull configuration. In contrast, **BNPXZ** shows the lowest  $\beta_{\text{tot}}$  ( $6.42 \times 10^{-30}$  esu) value. The dominant contributing tensor for **BTNC**, **BNTC**, **BNPZ** and **BNTF** is  $\beta_{xxx}$ , with magnitudes of  $3.71 \times 10^{-29}$ ,  $3.61 \times 10^{-29}$ ,  $-3.26 \times 10^{-29}$  and  $9.74 \times 10^{-29}$ , respectively. For **BNAC** and **BNPXZ**, the governing tensor is  $\beta_{xyy}$ , with values of  $-5.01 \times 10^{-31}$  and  $1.35 \times 10^{-29}$ , respectively. In contrast, in **BNTA**, and **BNTD**, the dominant contribution comes from  $\beta_{xyy}$ , with values of  $2.13 \times 10^{-29}$ , and  $2.08 \times 10^{-29}$ , respectively. The total second hyperpolarizability ( $\gamma_{\text{tot}}$ ) values for studied chromophores were also computed, as shown in Table S28.<sup>†</sup> For **BNTF**, which exhibits the highest  $\gamma_{\text{tot}}$  value ( $81.11 \times 10^{-35}$  esu) among all the compounds, the dominant contribution originates from the  $\gamma_x$  tensor ( $3.59 \times 10^{-34}$  esu) while the least contribution is attributed to the tensor  $\gamma_z$  ( $6.66 \times 10^{-36}$ ).

The frequency-dependent NLO properties for the compounds under investigation were calculated at the laser wavelengths of 532 nm ( $\omega = 0.042823$  a.u.) and 1064 nm ( $\omega = 0.085645$  a.u.) (Tables S30 and S31<sup>†</sup>). These properties include the electro-optic pockel's effect (EOPE),  $\beta(-\omega, \omega, 0)$ , and simple harmonic generation (SHG),  $\beta(-2\omega, \omega, \omega)$ , for first hyperpolarizabilities, as well as the electro-optic kerr effect (EOKO),

$\gamma(-\omega, \omega, 0, 0)$ , and electric field-induced second harmonic generation (ESHG),  $\gamma(-2\omega, \omega, \omega, 0)$ , for third-order responses. These parameters were evaluated to assess their potential for NLO applications. From the first hyperpolarizability values, summarized in Table S30,<sup>†</sup> it is evident that the EOPE and SHG are higher at 532 nm for most of the compounds. For example, at 532 nm, **BTNC** exhibited the first hyperpolarizability of  $\beta(-\omega, \omega, 0) = 2.78 \times 10^{-29}$  esu and  $\beta(-2\omega, \omega, \omega) = 7.31 \times 10^{-29}$  esu. In contrast, **BNTF** exhibited the highest static values among the synthesized compounds, highlighting its strong NLO response. The third-order responses displayed notable trends as well. **BNTF** showed the highest EOKO value at 532 nm, with  $\gamma(-\omega, \omega, 0, 0) = 1.19 \times 10^{-33}$  esu, indicating its strong potential for third-order NLO applications. Similarly, **BNPXZ** demonstrated remarkable ESHG values at 1064 nm, with  $\gamma(-2\omega, \omega, \omega, 0) = 3.89 \times 10^{-33}$  esu, showing its promise as a high-performance chromophore for second-order NLO processes. At 1064 nm, frequency-dependent properties were consistently enhanced for certain compounds. For instance, **BNPXZ** exhibited significant third-order NLO responses, with  $\gamma(-\omega, \omega, 0, 0) = 7.36 \times 10^{-33}$  esu, indicating its potential as a high-performance third-order NLO chromophore. These results demonstrate the wavelength dependence of NLO properties, suggesting that the compounds can be tailored for specific applications at both 532 nm and 1064 nm. Above data provide understanding of the electro-optic and harmonic generation potential of these molecules for specific applications in optoelectronics, telecommunication, and other advanced technologies.

## Conclusion

Herein, the optoelectronic and nonlinear optical (NLO) properties of BNCz based synthesized compounds namely **BTNC**–**BNAC** were explored. To explore the effect of  $\pi$ -conjugation (2-phenylthiophene) with various robust donors on the NLO properties, a set of four BNCz compounds (**BNTF**–**BNTD**) were designed. The effect of structural tailoring in the designed molecules was assessed for their NLO response using DFT computations. The D- $\pi$ -A framework in compounds **BNTF**–**BNTD** exhibited comparable electronic properties to those of the D-A (**BTNC**–**BNPZ**) configuration. The  $E_g$  of all the explored compounds is found to be lower (2.784–3.774 eV) accompanied by redshift in absorption (566.138–412.854 nm). The energy order follows the trend: **BTNC** > **BNAC** > **BNTC**  $\approx$  **BNTA** > **BNTF** > **BNPXZ** > **BNTD** > **BNPZ**. NBO analysis indicated that strong intramolecular interactions were key factors in stabilizing the studied compounds. Additionally, GRP analysis revealed higher softness, and lower hardness in all the entitled compounds especially in **BNPZ** and **BNTD**. These findings support the enhanced polarizability and charge transfer in the studied chromophores, leading to their suitable NLO properties. Among all the studied chromophores, the highest  $\beta_{\text{tot}}$  and  $\gamma_{\text{tot}}$  values were observed for **BNTF**, measuring ( $74.0 \times 10^{-30}$  esu) and  $\gamma_{\text{tot}}$  ( $81.1 \times 10^{-35}$  esu), respectively. This study offers insights into the structure-property relationship of the optoelectronic compounds and may encourage experimental researchers to synthesize them for their notable NLO characteristics.





## Data availability

All data generated or analyzed during this study are included in this published article and its ESI Files.†

## Conflicts of interest

There are no conflicts of interest to declare.

## Acknowledgements

The work was supported and funded by the Deanship of Scientific Research at Imam Mohammad Ibn Saud Islamic University (IMSIU) (grant number IMSIU-DDRSP 2503).

## References

- 1 F. Brown, R. E. Parks and A. M. Sleeper, *Phys. Rev. Lett.*, 1965, **14**, 1029.
- 2 P. Franken, A. E. Hill, C. e. Peters and G. Weinreich, *Phys. Rev. Lett.*, 1961, **7**, 118.
- 3 J. Lin and C. Chen, *Lasers Optron.*, 1987, **6**, 59–63.
- 4 S. Muhammad, S. Kumar, J. Koh, M. Saravanabhavan, K. Ayub and M. Chaudhary, *Mol. Simul.*, 2018, **44**, 1191–1199.
- 5 A. Wadsworth, M. Moser, A. Marks, M. S. Little, N. Gasparini, C. J. Brabec, D. Baran and I. McCulloch, *Chem. Soc. Rev.*, 2019, **48**, 1596–1625.
- 6 N. Liang, W. Jiang, J. Hou and Z. Wang, *Mater. Chem. Front.*, 2017, **1**, 1291–1303.
- 7 P. Cheng, G. Li, X. Zhan and Y. Yang, *Nat. Photonics*, 2018, **12**, 131–142.
- 8 S. R. Marder, J. E. Sohn and G. D. Stucky, *Materials for Nonlinear Optics: Chemical Perspectives*, ACS Publications, 1991.
- 9 V. Srinivasan, M. Panneerselvam, N. Pavithra, S. Anandan, K. Sundaravel, M. Jaccob and A. Kathiravan, *J. Photochem. Photobiol., A*, 2017, **332**, 453–464.
- 10 J.-L. Oudar and D. S. Chemla, *J. Chem. Phys.*, 1977, **66**, 2664–2668.
- 11 H. Alyar, *Rev. Adv. Mater. Sci.*, 2013, **34**, e87.
- 12 H. Narita, H. Min, N. Kubo, I. Hattori, T. Yasuda and S. Yamaguchi, *Angew. Chem., Int. Ed.*, 2024, e202405412.
- 13 B. Xerri, F. Labat, K. Guo, S. Yang and C. Adamo, *Theor. Chem. Acc.*, 2016, **135**, 1–9.
- 14 Y.-H. He, F.-M. Xie, H.-Z. Li, K. Zhang, Y. Shen, F. Ding, C.-Y. Wang, Y.-Q. Li and J.-X. Tang, *Mater. Chem. Front.*, 2023, **7**, 2454–2463.
- 15 M. Frisch, G. Trucks, H. Schlegel, G. Scuseria, M. Robb, J. Cheeseman, G. Scalmani, V. Barone, G. Petersson and H. Nakatsuji, *Gaussian 16*, Revision C.01, Gaussian, Inc., Wallingford, CT, 2016.
- 16 M. D. Hanwell, D. E. Curtis, D. C. Lonie, T. Vandermeersch, E. Zurek and G. R. Hutchison, *J. Cheminf.*, 2012, **4**, 1–17.
- 17 N. M. O'boyle, A. L. Tenderholt and K. M. Langner, *J. Comput. Chem.*, 2008, **29**, 839–845.
- 18 G. Zhurko, *Chemcraft*, 2014, <http://www.chemcraftprog.com>.
- 19 T. Lu and F. Chen, *J. Comput. Chem.*, 2012, **33**, 580–592.
- 20 R. Dennington, T. Keith and J. Millam, *GaussView 5.0*, Gaussian, Inc., Wallingford, 2008, 20.
- 21 J. C. Kromann, C. Steinmann and J. H. Jensen, *J. Chem. Phys.*, 2018, **149**, 104102.
- 22 A. Alparone, *Chem. Phys.*, 2013, **410**, 90–98.
- 23 A. Plaquet, M. Guillaume, B. Champagne, F. Castet, L. Ducasse, J.-L. Pozzo and V. Rodriguez, *Phys. Chem. Chem. Phys.*, 2008, **10**, 6223–6232.
- 24 F. Ullah, K. Ayub and T. Mahmood, *New J. Chem.*, 2020, **44**, 9822–9829.
- 25 S. Haq, M. A. Asghar, I. Shafiq, M. Saeed, W. Anwer, M. Haroon and R. Alotaibi, *Comput. Theor. Chem.*, 2024, **1240**, 114788.
- 26 I. Shafiq, M. Khalid, R. Jawaria, Z. Shafiq, M. Haroon and T. Ahamad, *J. Mol. Struct.*, 2025, **1326**, 141142.
- 27 R. G. Parr and R. G. Pearson, *J. Am. Chem. Soc.*, 1983, **105**, 7512–7516.
- 28 A. Luzanov and O. Prezhdo, *J. Chem. Phys.*, 2006, **124**, 224109.
- 29 R. G. Parr, L. v. Szentpály and S. Liu, *J. Am. Chem. Soc.*, 1999, **121**, 1922–1924.
- 30 K. Fukui, *Science*, 1982, **218**, 747–754.
- 31 R. G. Parr, R. A. Donnelly, M. Levy and W. E. Palke, *J. Chem. Phys.*, 1978, **68**, 3801–3807.
- 32 T. Koopmans, *Physica*, 1934, **1**, 104–113.
- 33 J. Padmanabhan, R. Parthasarathi, V. Subramanian and P. Chattaraj, *J. Phys. Chem. A*, 2007, **111**, 1358–1361.
- 34 M. U. Khan, M. Ibrahim, M. Khalid, S. Jamil, A. A. Al-Saadi and M. R. S. A. Janjua, *Chem. Phys. Lett.*, 2019, **719**, 59–66.
- 35 H. Mehmood, M. Haroon, T. Akhtar, S. Jamal, M. N. Akhtar, M. U. Khan and N. Alhokbany, *Synth. Met.*, 2024, **307**, 117701.
- 36 M. Khalid, I. Shafiq, M. Zhu, M. U. Khan, Z. Shafiq, J. Iqbal, M. M. Alam, A. A. C. Braga and M. Imran, *J. Saudi Chem. Soc.*, 2021, **25**, 101305.
- 37 N. Boukabcha, A. Djafri, Y. Megrouss, Ö. Tamer, D. Avci, M. Tuna, N. Dege, A. Chouaih, Y. Atalay and F. Hamzaoui, *J. Mol. Struct.*, 2019, **1194**, 112–123.
- 38 I. Shafiq, M. Khalid, M. A. Asghar, M. Adeel, M. F. ur Rehman, A. Syed, A. H. Bahkali, A. M. Elgorban and M. S. Akram, *J. Mater. Res. Technol.*, 2023, **24**, 1882–1896.
- 39 M. Ans, J. Iqbal, Z. Ahmad, S. Muhammad, R. Hussain, B. Eliasson and K. Ayub, *ChemistrySelect*, 2018, **3**, 12797–12804.
- 40 N. Tsutsumi, M. Morishima and W. Sakai, *Macromolecules*, 1998, **31**, 7764–7769.
- 41 M. N. Arshad, I. Shafiq, M. Khalid and A. M. Asiri, *ACS Omega*, 2022, **7**, 11606–11617.
- 42 A. Mahmood, A. Irfan, F. Ahmad and M. R. S. A. Janjua, *Comput. Theor. Chem.*, 2021, **1204**, 113387.
- 43 S. Bibi, R. Jia, H.-X. Zhang and F.-Q. Bai, *Sol. Energy*, 2019, **186**, 311–322.
- 44 S. Kraner, G. Prampolini and G. Cuniberti, *J. Phys. Chem. C*, 2017, **121**, 17088–17095.
- 45 İ. Sıdır, Y. G. Sıdır, M. Kumalar and E. Taşal, *J. Mol. Struct.*, 2010, **964**, 134–151.





- 46 M. Khalid, M. U. Khan, I. Shafiq, R. Hussain, A. Ali, M. Imran, A. A. Braga, M. Fayyaz ur Rehman and M. S. Akram, *R. Soc. Open Sci.*, 2021, **8**, 210570.
- 47 M. Szafran, A. Komasa and E. Bartoszak-Adamska, *J. Mol. Struct.*, 2007, **827**, 101–107.
- 48 A. Karakas, A. Elmali and H. Unver, *Spectrochim. Acta, Part A*, 2007, **68**, 567–572.
- 49 A. E. Reed, L. A. Curtiss and F. Weinhold, *Chem. Rev.*, 1988, **88**, 899–926.
- 50 J. L. Bredas, C. Adant, P. Tackx, A. Persoons and B. Pierce, *Chem. Rev.*, 1994, **94**, 243–278.
- 51 V. M. Geskin, C. Lambert and J.-L. Brédas, *J. Am. Chem. Soc.*, 2003, **125**, 15651–15658.
- 52 K. J. Miller, *J. Am. Chem. Soc.*, 1990, **112**, 8543–8551.

